

An Upwind Generalized Finite Difference Method for Meshless Solution of Two-phase Porous Flow Equations

Xiang Rao*, Yina Liu, Hui Zhao
Yangtze University

*Corresponding author: raoxiang0103@163.com

Abstract: This paper makes the first attempt to apply newly developed upwind GFDM for the meshless solution of two-phase porous flow equations. In the presented method, meshless nodes are flexibly collocated to characterize the computational domain, instead of complicated mesh generation, and the computational domain is divided into overlapping sub-domains centered on each node. Combining with moving least square approximation and local Taylor expansion, derivatives of oil-phase pressure at the central node are approximated by a generalized difference scheme of nodal pressure in the local subdomain. By introducing the upwind scheme of phase permeability, fully implicit nonlinear discrete equations of the immiscible two-phase porous flow are obtained and solved by Newton iteration method with automatic differentiation technology, to avoid the additional computational cost and possible computational instability caused by sequentially coupled scheme. The upwind GFDM with the fully implicit nonlinear solver given in this paper may provide a critical reference for developing a general-purpose meshless numerical simulator for porous flow.

Keywords: Generalized finite difference method; Multiphase flow in porous media; Meshless method; Upwind scheme;

1. Introduction

The meshless generalized finite difference method (GFDM) is a meshless method [1,2] developed in recent years. Based on the Taylor series expansion of multivariate functions in the subdomain and the weighted least squares approximation, the first-order and the second-order partial derivatives of the unknown function in the differential equation is expressed as a linear combination of nodal unknown values in the subdomain, which overcomes the dependence of the traditional finite difference method on the mesh division. At present, this method has developed rapidly and is widely used to solve various scientific and engineering problems, including shallow water equation [3], high-order partial differential equation [4], transient heat conduction analysis [5], stress analysis [6], water wave interaction [7], inverse heat source problem [8], seismic wave propagation problem [9], coupled thermoelasticity problem [10-12], stochastic analysis of groundwater flow [13], And some typical differential equation problems (e.g., unsteady Burger's equation [14-15], nonlinear convection difference equation [16], fractional diffusion equation [17]). In general, the generalized finite difference method only needs to arrange a group of nodes in the calculation domain to realize the accurate solution of the control equation, which can save the complicated meshing of the calculation domain with complex geometric features in finite element, finite difference, and boundary element methods and a large number of numerical integrals required in some meshless methods. Benito et al. proposed a self-adaptive GFDM, it realizes the automatic local node allocation according to the accuracy requirements [18]. On the one hand, these studies show that GFDM is an efficient and high-accuracy meshless numerical modeling method. On the other hand, since GFDM has theoretical advantages over traditional finite-difference or other mesh-based methods, the potential of GFDM (e.g., constructing a general GFDM-based simulator of physical field problems) has not been fully explored.

For the flow problem, it is often necessary to take an upwind scheme when dealing with some physical parameters in governing equations. In the meshless method, the upstream scheme is generally realized by modifying the influence domain of the allocation node, including the upwind influence domain [19] that moves the central node to the upstream direction and the partial influence domain [20] that more upstream nodes are included in the influence domain of the central node. However, because the actual flow field may be very complex, it is difficult to form a stable upwind effect by modifying the influence region, and satisfactory calculation accuracy is difficult to be effectively guaranteed. Rao et al. [21] pointed out that although the generalized finite difference method is meshless, it also has the characteristics of FDM. Therefore, GFDM can directly learn from the upwind scheme in FDM. Then an upwind GFDM is given without modifying the node influence domain, based on which, the high-accuracy modeling of single-phase heat and mass transfer is realized.

Rao et al. 's work [21] implies the great potential of upwind GFDM in porous media flow. Immiscible two-phase flow is a basic scenario of porous media flow, such as oil-water two-phase flow in an underground

reservoir [22]. The relative phase permeability in the two-phase flow equation is a typical physical parameter that needs to take the upwind scheme. To further verify the effectiveness of the application of upwind GFDM in porous media flow, this paper aims to explore the computational performances of upwind GFDM in two-phase porous flow, and solve the equations by using the fully implicit scheme and the nonlinear solver based on Newton iteration, so as to eliminate the additional computational cost and possible computational instability in the sequentially coupled scheme. Numerical examples in this paper validate the good computational performances of upwind GFDM for two-phase porous flow.

In all, the good computational performances of upwind GFDM in single-phase mass and heat coupled transfer and two-phase porous flow in this paper, as well as the successful application of the fully implicit coupling scheme suitable for governing equations of various porous flows, shows that based on upwind GFDM, a general meshless numerical simulator for flow in porous media may be formed, so as to provide a new numerical simulation technology for underground oil and gas reservoir development, geothermal resource development, groundwater flow, carbon-dioxide geological capture, environmental protection, etc.

2. Coupled governing equations in two-phase porous flow

Taking the immiscible oil-water two-phase flow in porous media as an example, the governing equations of the two-phase flow include the mass conservation equations of water phase and oil phase, and the auxiliary equations representing the relationship between the physical quantities in the mass conservation equation, respectively:

Mass conservation equations of oil phase:

$$0.0864\nabla \cdot \left(\frac{kk_{ro}}{\mu_o} \nabla p_o \right) + q_o = \frac{\partial(\phi S_o)}{\partial t} \quad (1)$$

where, k is permeability, mD; $k_{ro} = k_{ro}(S_w)$ is the relative permeability of oil phase, which is a function of water saturation S_w ; μ_o is the oil phase viscosity, mPa·s; p_o is the oil phase pressure, MPa; q_o is the source or sink item of oil phase, 1/day; t is time, day; $\phi = \phi(p)$ is the reservoir porosity which is a function of pressure, fraction; S_o is oil saturation; The unit of length is meters.

Mass conservation equations of water phase:

$$0.0864\nabla \cdot \left(\frac{kk_{rw}}{\mu_w} \nabla p_w \right) + q_w = \frac{\partial(\phi S_w)}{\partial t} \quad (2)$$

where, $k_{rw} = k_{rw}(S_w)$ is the relative permeability of water phase, which is a function of water saturation; μ_w is the water phase viscosity, mPa·s; p_w is the water phase pressure, MPa; q_w is the source or sink item of water phase, 1/day;

Auxiliary equations:

The basic variables in the above two equations are generally selected as oil phase pressure p_o and water saturation S_w . The functional relationship between other physical quantities and the two basic variables is as follows:

$$S_o = 1 - S_w, \quad p_w = p_o - P_c(S_w), \quad \phi = \phi(p_o) = \phi_0 + C_r(p_o - p_o^0), \quad k_{rw} = k_{rw}(S_w), \quad k_{ro} = k_{ro}(S_w) \quad (3)$$

where, $C_t = C_t(S_w)$ is the comprehensive compressibility coefficient, 1/MPa; p_o^0 is the original oil phase pressure and ϕ_0 is the corresponding porosity; $\phi = \phi(p)$ is porosity which is a function of oil phase pressure; $k_{rw} = k_{rw}(S_w)$ and $k_{ro} = k_{ro}(S_w)$ are the relative permeabilities of water phase and oil phase which are functions of water saturation. Therefore, Eq. (1) and Eq. (2) constitute a nonlinear system about p_o and S_w .

3. Meshless upwind GFDM for the two-phase porous flow problems

GFDM is a meshless collocation method developed rapidly in recent years. By using local Taylor expansion and moving least squares in the node influence domain, the approximate scheme of each order partial derivative of unknown variables at the node is obtained. The approximate scheme is a linear combination of the unknown variable values of each node in the influence domain of the node, which is similar to the difference expression in the FDM, so it is called GFDM.

For a node $M_0 = (x_0, y_0)$ in the computing domain, suppose another n nodes are contained in the influence domain of the node, which is denoted as $\{M_1, M_2, M_3, \dots, M_n\}$, where $M_i = (x_i, y_i)$. Take Taylor expansion of $\{u(M_i), i = 1, \dots, n\}$ at the node $M_0 = (x_0, y_0)$ to obtain:

$$u|_{M_i} = u|_{M_0} + \Delta x_i u_x|_{M_0} + \Delta y_i u_y|_{M_0} + \frac{1}{2} \left((\Delta x_i)^2 u_{xx}|_{M_0} + \Delta x_i \Delta y_i u_{xy}|_{M_0} + (\Delta y_i)^2 u_{yy}|_{M_0} \right) + o(\Delta x_i^2, \Delta y_i^2) \quad (4)$$

where $\Delta x_i = x_0 - x_i$, $\Delta y_i = y_0 - y_i$.

It can be seen that the closer $M_i = (x_i, y_i)$ is to the central node $M_0 = (x_0, y_0)$, the right side of Eq. (4) after removing the remainder should be more valid. Therefore, define the weighted error function in Eq. (5), in which the closer the distance, the greater the weight.

$$B(\mathbf{D}_u) = \sum_{j=1}^n \left[\left(u_0 - u_j + \Delta x_j u_x|_{M_0} + \Delta y_j u_y|_{M_0} + \frac{1}{2} (\Delta x_j)^2 u_{xx}|_{M_0} + \frac{1}{2} (\Delta y_j)^2 u_{yy}|_{M_0} + \Delta x_j \Delta y_j u_{xy}|_{M_0} \right) \omega_j \right]^2 \quad (5)$$

where, $\mathbf{D}_u = \left(u_x|_{M_0}, u_y|_{M_0}, u_{xx}|_{M_0}, u_{yy}|_{M_0}, u_{xy}|_{M_0} \right)^T$, $\omega_j = \omega(\Delta x_j, \Delta y_j)$ is the weight function. Fan and Li [14] demonstrated that different types of weight functions have little impact on the calculation results, while the quartic spline function in Eq. (6) is generally selected to calculate the weight in Eq. (5):

$$\omega_j = \begin{cases} 1 - 6 \left(\frac{r_j}{r_m} \right)^2 + 8 \left(\frac{r_j}{r_m} \right)^3 - 3 \left(\frac{r_j}{r_m} \right)^4 & r_j \leq r_m \\ 0 & r_j > r_m \end{cases} \quad (6)$$

where $r_j = \sqrt{\Delta x_j^2 + \Delta y_j^2}$ is the Euclidean distance from node M_j to node M_0 , r_m is the radius of the node influence domain.

Based on the moving least squares, the minimum value of $B(\mathbf{D}_u)$ is required, then the partial derivatives of $B(\mathbf{D}_u)$ with respect to each component in the independent variable \mathbf{D}_u should be equal to zero, these are,

$$\frac{\partial B(\mathbf{D}_u)}{\partial u_x|_{M_0}} = 0, \frac{\partial B(\mathbf{D}_u)}{\partial u_y|_{M_0}} = 0, \frac{\partial B(\mathbf{D}_u)}{\partial u_{xx}|_{M_0}} = 0, \frac{\partial B(\mathbf{D}_u)}{\partial u_{yy}|_{M_0}} = 0, \frac{\partial B(\mathbf{D}_u)}{\partial u_{xy}|_{M_0}} = 0 \quad (7)$$

Eq. (7) is sorted into linear equations as follows:

$$\mathbf{A} \mathbf{D}_u = \mathbf{b} \quad (8)$$

where $\mathbf{A} = \mathbf{L}^T \boldsymbol{\omega} \mathbf{L}$, $\mathbf{b} = \mathbf{L}^T \boldsymbol{\omega} \mathbf{U}$, $\mathbf{L} = (\mathbf{L}_1^T, \mathbf{L}_2^T, \dots, \mathbf{L}_n^T)^T$, $\mathbf{L}_i = \left(\Delta x_i, \Delta y_i, \frac{\Delta x_i^2}{2}, \frac{\Delta y_i^2}{2}, \Delta x_i \Delta y_i \right)$, $\boldsymbol{\omega} = \text{diag}(\omega_1^2, \omega_2^2, \dots, \omega_n^2)$,

$\mathbf{U} = (u_1 - u_0, u_2 - u_0, \dots, u_n - u_0)^T$.

Then it is obtained that,

$$\mathbf{D}_u = (u_{x0}, u_{y0}, u_{xx0}, u_{yy0}, u_{xy0})^T = \mathbf{A}^{-1} \mathbf{b} = \mathbf{A}^{-1} \mathbf{L}^T \boldsymbol{\omega} \mathbf{U} = \mathbf{E} \mathbf{U} \quad (9)$$

where $\mathbf{E} = \mathbf{A}^{-1} \mathbf{L}^T \boldsymbol{\omega}$.

Thus, the approximate scheme of the first-order and second-order partial derivatives at the central node are:

$$\begin{aligned} u_x|_{M_0} &= \sum_{j=1}^n e_{1j} (u|_{M_j} - u|_{M_0}), & u_y|_{M_0} &= \sum_{j=1}^{n+1} e_{2j} (u|_{M_j} - u|_{M_0}), & u_{xx}|_{M_0} &= \sum_{j=1}^{n+1} e_{3j} (u|_{M_j} - u|_{M_0}), \\ u_{yy}|_{M_0} &= \sum_{j=1}^{n+1} e_{4j} (u|_{M_j} - u|_{M_0}), & u_{xy}|_{M_0} &= \sum_{j=1}^{n+1} e_{5j} (u|_{M_j} - u|_{M_0}) \end{aligned} \quad (10)$$

where e_{ij} is the element of matrix \mathbf{E} .

Therefore, GFDM can obtain the approximation of the first-order derivative and the second-order derivative at the central node according to the coordinates of nodes in the influence domain of the central node, and can iteratively obtain the approximation of the higher-order derivative at the central node, so that the discretization of the governing differential equation of physical field can be realized without complex mesh generation when only the nodes are allocated in the computational domain. For the computational domain with complex geometry, meshless GFDM has better adaptability than the finite difference method based on mesh generation (including finite element method, finite volume method, etc.).

Although the GFDM is a meshless method, it also has the characteristics of FDM. so GFDM can directly learn from the upwind scheme in FDM. Then, an upwind GFDM can realize a stable upwind effect without modifying the node influence domain, which can detailly refer to Rao's work.

In this paper, the fully implicit coupling scheme is used to discretize the governing equations, in which the node pressure and saturation at the time $t + \Delta t$ are solved simultaneously. It may be assumed that the source or sink term is zero, the discrete scheme of oil-phase and water-phase equations based on GFDM is as follows:

$$0.0864 \sum_{j=1}^{n_i} \left[\frac{k_{ij}^{t+\Delta t} k_{ro,ij}^{t+\Delta t}}{\mu_{o,ij}^{t+\Delta t}} (e_{3,j}^i + e_{4,j}^i) (p_{o,(i,j)}^{t+\Delta t} - p_{o,i}^{t+\Delta t}) \right] = \frac{1}{\Delta t} \left[(\phi_i^{t+\Delta t} S_{o,i}^{t+\Delta t}) - (\phi_i^t S_{o,i}^t) \right] \quad (11)$$

$$0.0864 \sum_{j=1}^{n_i} \left[\frac{k_{ij}^{t+\Delta t} k_{rw,ij}^{t+\Delta t}}{\mu_{w,ij}^{t+\Delta t}} (e_{3,j}^i + e_{4,j}^i) (p_{o,(i,j)}^{t+\Delta t} - p_{o,i}^{t+\Delta t} + P_{c,(i,j)}^{t+\Delta t} - P_{c,i}^{t+\Delta t}) \right] = \frac{[\phi_i^{t+\Delta t} (1 - S_{o,i}^{t+\Delta t}) - \phi_i^t (1 - S_{o,i}^t)]}{\Delta t} \quad (12)$$

where $\phi_i^{t+\Delta t} = \phi(p_{o,i}^{t+\Delta t})$, $\phi_i^t = \phi(p_{o,i}^t)$, $P_{c,(i,j)}^{t+\Delta t} = P_c(S_{w,(i,j)}^{t+\Delta t})$, $P_{c,i}^{t+\Delta t} = P_c(S_{w,i}^{t+\Delta t})$. Permeability $k_{ij}^{t+\Delta t}$ and viscosity $\mu_{w,ij}^{t+\Delta t}$ adopt harmony average scheme and arithmetic average scheme, respectively, these are:

$$k_{ij}^{t+\Delta t} = \frac{2}{1/k_i^{t+\Delta t} + 1/k_j^{t+\Delta t}}, \quad \mu_{o,ij}^{t+\Delta t} = \frac{\mu_{o,i}^{t+\Delta t} + \mu_{o,j}^{t+\Delta t}}{2}, \quad \mu_{w,ij}^{t+\Delta t} = \frac{\mu_{w,i}^{t+\Delta t} + \mu_{w,j}^{t+\Delta t}}{2} \quad (13)$$

Eq. (14) gives the upwind scheme of oil phase and water phase relative permeability. It can be seen that the upwind GFDM can obtain the upwind effect without modifying the node influence region, which is also a significant feature of the upwind GFDM different from the original GFDM and other meshless methods.

$$k_{ro,ij}^{t+\Delta t} = \begin{cases} k_{ro,i}(S_{w,i}^{t+\Delta t}) & \text{if } p_{o,(i,j)}^{t+\Delta t} \geq p_{o,i}^{t+\Delta t} \\ k_{ro,i}(S_{w,i}^{t+\Delta t}) & \text{if } p_{o,(i,j)}^{t+\Delta t} < p_{o,i}^{t+\Delta t} \end{cases}, \quad k_{rw,ij}^{t+\Delta t} = \begin{cases} k_{rw}(S_{w,(i,j)}^{t+\Delta t}) & \text{if } p_{o,(i,j)}^{t+\Delta t} \geq p_{o,i}^{t+\Delta t} \\ k_{rw}(S_{w,i}^{t+\Delta t}) & \text{if } p_{o,(i,j)}^{t+\Delta t} < p_{o,i}^{t+\Delta t} \end{cases} \quad (14)$$

It should be noted that in this paper, the derivative boundary conditions in the calculation domain are treated by adding virtual nodes outside the boundary. For details, please refer to the literature [26]. The brief introduction is as follows: in the calculation domain, suppose there are n_1 internal nodes, n_2 nodes with Dirichlet boundary conditions, and n_3 nodes with derivative boundary conditions. For a node A with the derivative boundary condition, suppose the sequence number of node A in all nodes be a , and the added virtual node corresponding to node A be recorded as node B . Since each derivative boundary condition node needs to add a corresponding virtual node, the number of nodes in the whole calculation domain has $n_1 + n_2 + n_3 + n_3$ nodes. Let the sequence number of virtual node B in all nodes be b , then the equation at node A is no longer the equation corresponding to the boundary condition, but the Eq. (25) which is the same as the Eq. (19) at an internal node. The equation subject to the boundary condition is used as the equation at the virtual node B . Finally, a system of equations composed of $2(n_1 + n_2 + n_3 + n_3)$ equations, including $2n_1$ Eq. (19)s, $2n_2$ Eq. (24)s, $2n_3$ Eq. (25)s and $2n_3$ Eq. (26)s. In this paper, Newton iteration method and automatic differentiation technology are used to obtain a stable solution of the fully coupled implicit nonlinear equations [22, 23]. Then the pressure and water saturation values of all nodes (including n_1 inner nodes, $n_2 + n_3$ boundary nodes and n_3 virtual nodes) at time $t + \Delta t$ are solved to avoid the additional calculation cost of small time steps which is adopted to ensure the numerical stability and accuracy in the sequentially coupled scheme.

3. Numerical cases

In this section, a test case of oil-water two-phase porous flow in a regular rectangular computational domain is designed. Firstly, the good calculation performances of upwind GFDM in this paper are verified under Cartesian node collocation, Then, an example through the flexible node collocation in the rectangular domain to achieve effective computing, and an example with an irregular computing domain, show the advantages of the upwind GFDM that, the meshless upwind GFDM can describe the computational domain through flexible node collocation without complex mesh generation.

3.1 validation of the presented method

This example selects a regular rectangular computational domain ($[0m, 200m] \times [0m, 80m]$), suppose the left boundary and right boundary (denoted as Γ_1 and Γ_2 , respectively) meet the first type of boundary conditions, and the upper boundary and lower boundary (denoted as Γ_3 and Γ_4 , respectively) meet closed boundary conditions, and the source or sink term is zero. Table 1 shows the values of physical parameters, and Eq. (14) summarizes the governing equations with initial and boundary conditions.

In this example, the FDM calculation results obtained with small space steps and small time steps ($\Delta x = 1m$, $\Delta y = 1m$, $\Delta t = 0.005d$) are used as reference solutions. Fig. 1 compares the calculation results of FDM ($\Delta x = 4m$, $\Delta y = 4m$) and upwind GFDM with radius of node influence domain $r_e = 1.001\sqrt{\Delta x^2 + \Delta y^2}$ on one-dimensional (1D) section $y = 40m$. It can be seen that upwind GFDM can basically achieve high accuracy, especially in pressure calculation. Only at the discontinuous water drive front, the calculation accuracy of water saturation is relatively low, but it is also satisfactory.

Then, select different radius of the node influence domain ($2.001\sqrt{\Delta x^2 + \Delta y^2}$, $3.001\sqrt{\Delta x^2 + \Delta y^2}$) in the upwind

GFDM. Fig. 2 visually compares the water saturation and pressure calculation results of the reference solution, FDM solution and upwind GFDM with different radius of the node influence domain. Table 2 quantitatively compares the relative errors (RE) of computational results. It can be seen that the computational relative errors of various methods for pressure satisfying the diffusion equation are small. For water saturation, the calculation accuracy of upwind GFDM with the radius of influence domain $r_e = 1.001\sqrt{\Delta x^2 + \Delta y^2}$ is comparable to that of upwind FDM. With the increase of the radius of the influence domain, the calculation error of upwind GFDM on water saturation decreases slightly. This can also be seen from the water saturation profiles in Fig. 2. With the increase of the radius of influence domain, the dissipation error at the discontinuity of water saturation front increases, However, the calculation error is still not much higher than FDM. The comparison results show that the upwind GFDM can almost achieve the calculation effect of upwind FDM under the same node/grid density. However, the upwind GFDM in this paper is a meshless method, which can be effectively applied to the calculation domain with complex geometry, while the actual underground reservoir where porous flow happens often has complex geometric characteristics (faults, complex boundaries, fractures, etc.). So, the comparisons show the great application potential of upwind GFDM in porous flow.

Considering that a general numerical simulator often requires a fully implicit scheme of governing equations, this paper adopts a fully implicit nonlinear solver based on Newton iteration and automatic differentiation. Table 3 compares the Newton iteration steps under different radius of node influence domains. It can be seen that the Newton iteration steps under different radius of node influence domain are the same, that is, the increase of the radius of the influence domain does not increase the nonlinearity of the system, indicating that different node influence domains can be flexibly selected in the actual calculation. In all, the results of this example provide a basis for constructing a robust and general numerical simulator of porous flow based on upwind GFDM.

Table 1 Physical parameters used in example 1

Parameter	Value	Parameter	Value
Permeability k	100 mD	Initial water saturation	0.2
Initial porosity ϕ_0	0.3	Irreducible water saturation S_{wc}	0.2
Rock compressibility C_r	0 MPa ⁻¹	Residual Oil Saturation S_{or}	0.2
Oil viscosity	5 mPa·s	Tolerated max time step size	20 days
Water viscosity	1 mPa·s	Initial time step size	0.01 day
Initial pressure	10 MPa	Tolerated error	10 ⁻⁶

$$0.0864\nabla \cdot \left(\frac{kk_{ro}}{\mu_o} \nabla p_o \right) = \frac{\partial(\phi S_o)}{\partial t}, \quad 0.0864\nabla \cdot \left(\frac{kk_{rw}}{\mu_w} \nabla p_w \right) = \frac{\partial(\phi S_w)}{\partial t},$$

$$k_{rw} = \left(\frac{S_w - S_{wc}}{1 - S_{or} - S_{wc}} \right)^2, \quad k_{ro} = \left(\frac{1 - S_w - S_{or}}{1 - S_{wc} - S_{or}} \right)^2, \quad p_0 = 10, \quad S_w = 0.8, \quad (15)$$

$$p|_{\Gamma_1} = 15, \quad p|_{\Gamma_2} = 10, \quad \frac{\partial p}{\partial y}|_{\Gamma_3} = 0, \quad \frac{\partial p}{\partial y}|_{\Gamma_4} = 0, \quad S_w|_{\Gamma_1} = 0.8, \quad S_w|_{\Gamma_2} = 0.2, \quad \frac{\partial S_w}{\partial y}|_{\Gamma_3} = 0, \quad \frac{\partial S_w}{\partial y}|_{\Gamma_4} = 0$$

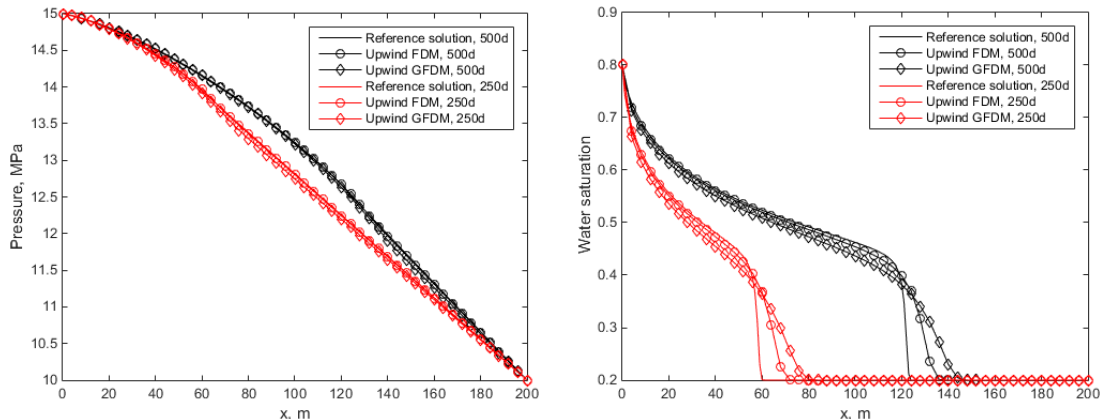


Fig. 1 Comparison of calculation results of oil-phase pressure and water saturation on $y = 40\text{m}$ section

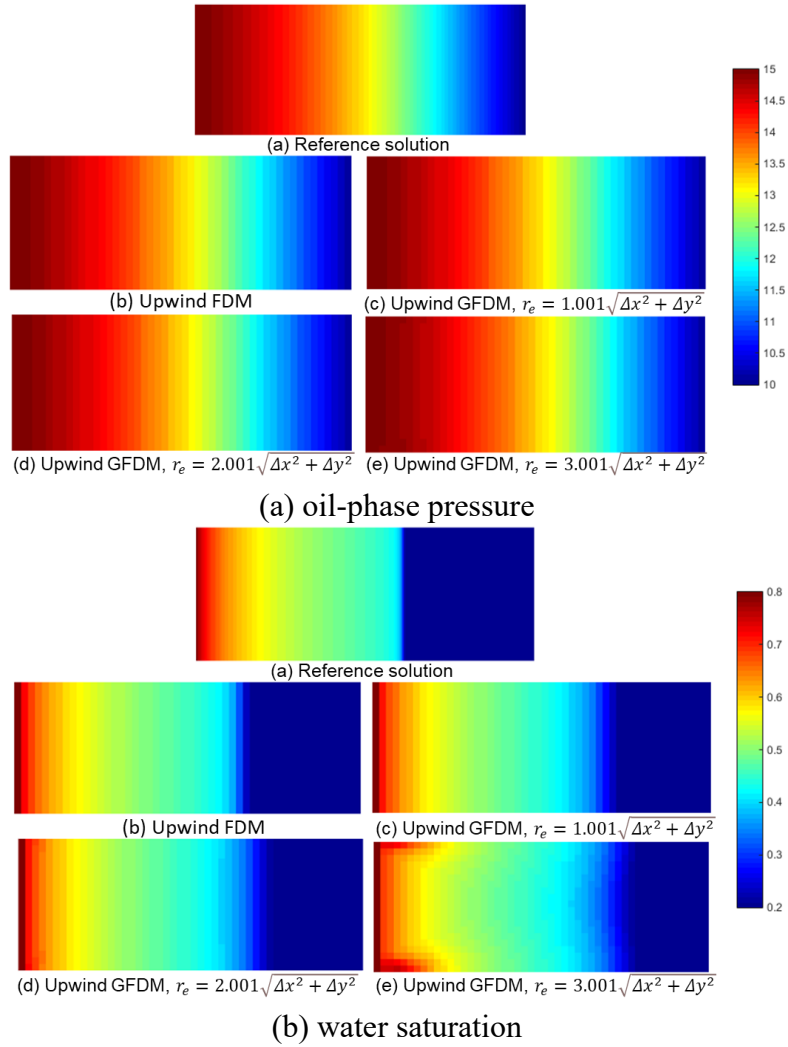


Fig. 2 Comparison of calculated pressure and water saturation profiles

Table 2 computational relative errors

Methods	FDM	Upwind GFDM $r_e = 1.001\sqrt{\Delta x^2 + \Delta y^2}$	Upwind GFDM $2.001\sqrt{\Delta x^2 + \Delta y^2}$	Upwind GFDM $3.001\sqrt{\Delta x^2 + \Delta y^2}$
RE of pressure (250 d)	0.0677%	0.2734%	0.2717%	0.2078%
RE of pressure (500 d)	0.0907%	0.2050%	0.1989%	0.2800%
RE of water saturation (250 d)	3.3082%	5.8095%	6.2752%	8.3986%
RE of water saturation (500 d)	3.9042%	7.1583%	7.7171%	10.6518%

Table 3 Newton iterations in case of different radius of node influential domain

Radius of influential domain	$1.001\sqrt{\Delta x^2 + \Delta y^2}$	$2.001\sqrt{\Delta x^2 + \Delta y^2}$	$3.001\sqrt{\Delta x^2 + \Delta y^2}$
Newton iterations	120	120	120

3.2 The significant advantage: flexible node collocation

Section 3.1 demonstrates that upwind GFDM can obtain calculation results with satisfactory accuracy, and the change of the radius of node influence domain has a limited impact on calculation accuracy. Therefore, compared with the FDM, finite element method (FEM) or finite volume method (FVM) that rely on high-quality mesh generation, the meshless upwind GFDM can discrete the complex geometry of the computational domain by using flexible node allocation, which greatly reduces the difficulty of pre-processing of computation.

As shown in Fig. 3 (a), for the computational domain in Section 3.1, this section first adopts a more flexible node allocation instead of the regular Cartesian node collocation. Fig. 4 shows the calculated pressure and water saturation profiles. It can be seen that the calculation results basically match the results in Fig. 2, which shows that the upwind GFDM in this paper can realize effective calculation under irregular node allocation. Then, this section gives a computational domain with irregular boundary shape and corresponding node

allocation as shown in Fig. 3 (b). The initial and boundary value conditions and governing equations are the same as those in Section 3.1, except that the shapes of the boundary Γ_1 and Γ_2 are different from those in Section 1. Fig. 5 shows the calculated water saturation and pressure profiles that look in line with physics, and it shows that the upwind GFDM in this paper can effectively calculate the two-phase porous flow through flexible node allocation in the case of the computational domain with complex geometry.

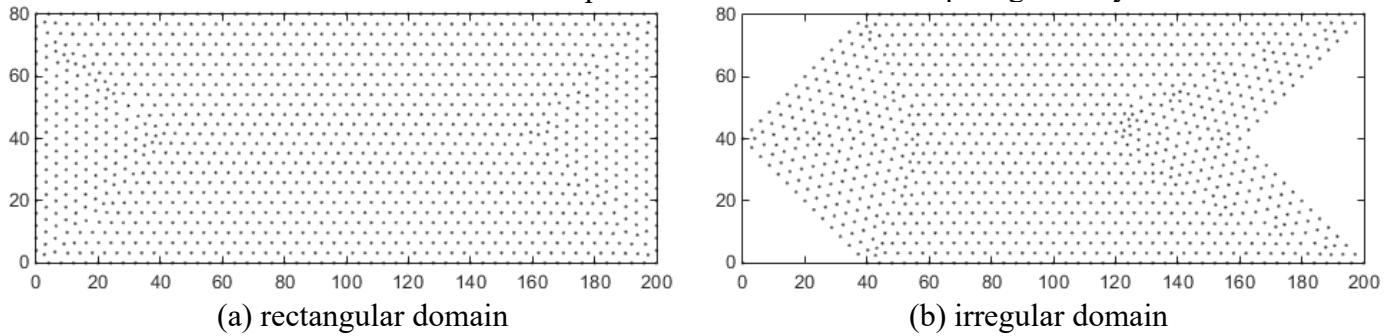


Fig. 3 sketch of computational domain

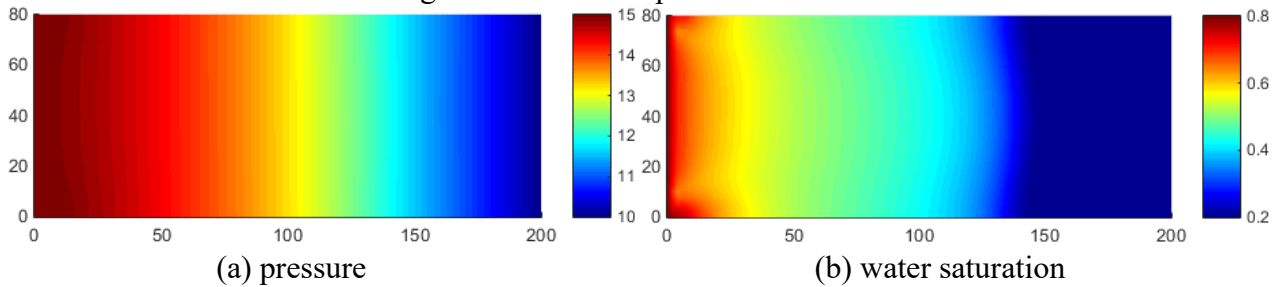


Fig. 4 calculation results in case of irregular node allocation

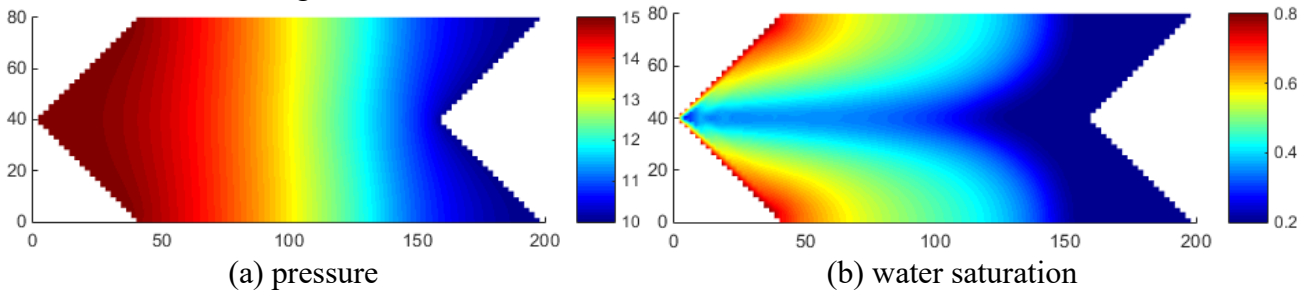


Fig. 5 calculation results in case of irregular boundary shape of the computational domain

4. Conclusions and future work

In this paper, upwind GFDM is first applied to two-phase porous flow equations, and realizes high-accuracy meshless calculation. Compared with the traditional mesh-based methods, this method uses meshless allocation nodes to describe the computational domain, avoids the difficulty of high-quality mesh generation, and has the advantages of more flexibility and simplicity in dealing with the computational domain with complex geometry. The results of this paper further verify the effectiveness of upwind GFDM and enrich the application scenario of upwind GFDM in porous flow. The upwind GFDM based single-phase heat and mass transfer and this study reveal that upwind GFDM may achieve good and stable computational performance in various porous flow problems. Therefore, based on upwind GFDM, it is possible to form a general meshless numerical simulator, which is valuable future work.

5. Acknowledgements

Dr. Rao thanks the supports from the National Natural Science Foundation of China (Nos. 52104017, 51874044, 51922007).

6. References

- [1] J.J. Benito, F. Urena, L. Gavete, Influence of several factors in the generalized finite difference method, *Appl. Math. Model.* 25 (12) (2001) 1039–1053.
- [2] Gavete L, Gavete M L, Benito J J. Improvements of generalized finite difference method and comparison with other meshless method[J]. *Applied Mathematical Modelling*, 2003, 27(10): 831-847.
- [3] P.-W. Li, C.-M. Fan, Generalized finite difference method for two-dimensional shallow water equations, *Eng. Anal. Bound. Elem.* 80 (2017) 58–71.

- [4] Urena F, Salete E, Benito J J, et al. Solving third- and fourth-order partial differential equations using GFDM: application to solve problems of plates[J]. *International Journal of Computer Mathematics*, 2012, 89(3): 366-376.
- [5] W. Qu, H. He, A spatial-temporal GFDM with an additional condition for transient heat conduction analysis of FGMs, *Appl. Math. Lett.* 110 (2020) 106579.
- [6] Y. Wang, Y. Gu, C.-M. Fan, W. Chen, C. Zhang, Domain-decomposition generalized finite difference method for stress analysis in multi-layered elastic materials, *Eng. Anal. Bound. Elem.* 94 (2018) 94–102.
- [7] Z.-J. Fu, Z.-Y. Xie, S.-Y. Ji, C.-C. Tsai, A.-L. Li, Meshless generalized finite difference method for water wave interactions with multiple-bottom-seated-cylinder-array structures, *Ocean Eng.* 195 (2020) 106736.
- [8] Gu Yan, Wang Lei, Chen Wen, et al. Application of the meshless generalized finite difference method to inverse heat source problems[J]. *International Journal of Heat and Mass Transfer*, 2017, 108(A): 721-729.
- [9] J.J. Benito, F. Ureña, L. Gavete, E. Salete, M. Ureña, Implementations with generalized finite differences of the displacements and velocity-stress formulations of seismic wave propagation problem, *Appl. Math. Model.* 52 (2017) 1–14.
- [10] H Xia, and Y. Gu . "Generalized finite difference method for electroelastic analysis of three-dimensional piezoelectric structures." *Applied Mathematics Letters* 117.2(2021):107084.
- [11] H. Xia, Y. Gu, Short communication: The generalized finite difference method for electroelastic analysis of 2D piezoelectric structures, *Eng. Anal. Bound. Elem.* 124 (2021) 82–86.
- [12] Y. Gu, W. Qu, W. Chen, L. Song, C. Zhang, The generalized finite difference method for long-time dynamic modeling of three-dimensional coupled thermoelasticity problems, *J. Comput. Phys.* 384 (2019) 42–59.
- [13] Syc, A, A. Kch , and B. Cmf . "Improvement of generalized finite difference method for stochastic subsurface flow modeling - ScienceDirect." *Journal of Computational Physics* (2020).
- [14] C.M. Fan, P.W. Li, Generalized finite difference method for solving two-dimensional Burgers' equations, *Proc. Eng.* 79 (2014) 55–60.
- [15] P.-W. Li, Space-time generalized finite difference nonlinear model for solving unsteady Burgers' equations, *Appl. Math. Lett.* 114 (2021) 106896.
- [16] Z.-J. Fu, Z.-C. Tang, H.-T. Zhao, P.-W. Li, T. Rabczuk, Numerical solutions of the coupled unsteady nonlinear convection–diffusion equations based on generalized finite difference method, *Eur. Phys. J. Plus* 134 (6) (2019) 272.
- [17] Gu Y, Sun HG. A meshless method for solving three-dimensional time fractional diffusion equation with variable-order derivatives. *Applied Mathematical Modelling*, 2020, 78: 539-549
- [18] J.J. Benito, F. Urena, L. Gavete, R. Alvarez, An h-adaptive method in the generalized finite differences, *Comput. Methods Appl. Mech. Engrg.* 192 (5–6) (2003) 735–759.
- [19] Atluri, S. N. , and S. Shen . "The Meshless Local Petrov-Galerkin (MLPG) Method: A Simple & Less-costly Alternative to the Finite Element and Boundary Element Methods." *Computer Modeling in Engineering and Sciences* 3.1(2002).
- [20] Cheng, M. , and G. R. Liu . "A novel finite point method for flow simulation." *International Journal for Numerical Methods in Fluids* 39.12(2002):1161-1178.
- [21] Rao X, Zhao H, et al. An Upwind General Finite Difference Method (GFDM) and Its Modeling of Heat and Mass Transfer in Porous Media, *Applied Mathematics and Computation*, 2021.
- [22] Rao X, Cheng L, Cao R, et al. A modified projection-based embedded discrete fracture model (pEDFM) for practical and accurate numerical simulation of fractured reservoir[J]. *Journal of Petroleum Science and Engineering*, 2020, 187: 106852.
- [23] Rao X, Xin L, H, Zhao H, et al. Numerical simulation of two-phase heat and mass transfer in fractured reservoirs based on projection-based embedded discrete fracture model (pEDFM), *Journal of Petroleum Science and Engineering*, 2022, 109323.